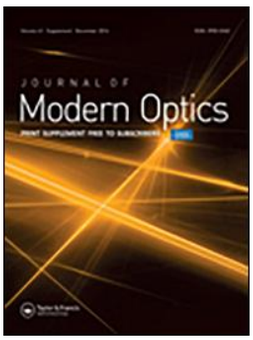

Journal of Modern Optics

ISSN: 0950-0340 (Print) 1362-3044 (Online) Journal homepage: https://www.tandfonline.com/loi/tmop20

Implications of stimulated resonant X-ray scattering for spectroscopy, imaging, and diffraction in the regime from soft to hard X-rays

Simon Schreck, Martin Beye & Alexander Föhlisch

To cite this article: Simon Schreck, Martin Beye & Alexander Föhlisch (2015) Implications of stimulated resonant X-ray scattering for spectroscopy, imaging, and diffraction in the regime from soft to hard X-rays, Journal of Modern Optics, 62:sup2, S34-S45, DOI: 10.1080/09500340.2015.1052028

To link to this article: https://doi.org/10.1080/09500340.2015.1052028

Published online: 17 Jul 2015.

Journal of Modern Optics, 2015
Vol. 62, No. S2, S34–S45, http://dx.doi.org/10.1080/09500340.2015.1052028

Taylor & Francis
Taylor & Francis Group

Implications of stimulated resonant X-ray scattering for spectroscopy, imaging, and diffraction in the regime from soft to hard X-rays

Simon Schreck[a,b1*], Martin Beye[a] and Alexander Föhlisch[a,b]

[a] *Institute for Methods and Instrumentation for Synchrotron Radiation Research, Helmholtz-Zentrum Berlin für Materialien und Energie GmbH, Berlin, Germany;* [b] *Institut für Physik und Astronomie, Universität Potsdam, Potsdam, Germany*

(*Received 18 February 2015; accepted 1 May 2015*)

The ultrahigh peak brilliance available at X-ray free-electron lasers opens the possibility to transfer nonlinear spectroscopic techniques from the optical and infrared into the X-ray regime. Here, we present a conceptual treatment of nonlinear X-ray processes with an emphasis on stimulated resonant X-ray scattering as well as a quantitative estimate for the scaling of stimulated X-ray scattering cross sections. These considerations provide the order of magnitude for the required X-ray intensities to experimentally observe stimulated resonant X-ray scattering for photon energies ranging from the extreme ultraviolet to the soft and hard X-ray regimes. At the same time, the regime where stimulated processes can safely be ignored is identified. With this basis, we discuss prospects and implications for spectroscopy, scattering, and imaging experiments at X-ray free-electron lasers.

Keywords: X-ray scattering; nonlinear X-ray spectroscopy

1. Introduction

When an intense electromagnetic light field propagates through a medium, the induced polarization may change nonlinearly with the strength of the external light field [1]. Deviations from the linear response typically occur, when the electromagnetic field strength becomes comparable to the Coulomb field inside the atoms or molecules of the medium. At optical frequencies, only laser light is intense enough to induce such a nonlinear response of the polarization of the medium. Accordingly, nonlinear optical processes were first observed shortly after the invention of the laser (which itself is based on the nonlinear optical process of stimulated emission) – in 1961 Franken et al. [2] observed the generation of higher harmonics of a ruby laser focused into a quartz crystal. This experiment is often taken as the beginning of nonlinear optics. In the following, a wealth of nonlinear optical processes was observed and is now employed routinely. One application is to generate intense and tunable (with variable frequency, pulse duration, or polarization) laser light. At the same time many different nonlinear optical spectroscopies have been developed, and provide selective probes of structure and dynamics of atoms, molecules, and materials [3,4]. High harmonic generation and spectroscopy, sum and difference frequency generation, stimulated Raman scattering, and four-wave mixing are some of the most widely applied techniques.

At X-ray frequencies, the interaction of electromagnetic fields with matter has been restricted to the linear regime for long time. On one hand, this was due to the lack of intense enough X-ray sources in combination with the generally low interaction cross section at X-ray frequencies. On the other hand, the involved excited state lifetimes are ultrashort. In general, X-rays are able to excite strongly bound core-level electrons yielding atomic centers with core-level vacancies (core holes). The lifetime of these highly excited states is on the femtosecond timescale as a result of ultrafast spontaneous core-hole relaxation processes. The short lifetime hinders the creation of a sufficiently dense population inversion, which is needed for typical nonlinear processes such as stimulated emission. In particular, for the soft X-ray regime nonradiative core-hole relaxation via the Auger process plays an important role. Highly energetic Auger electrons are created that can significantly alter the geometric and electronic structure of the sample at high incident X-ray intensities [5–7].

However, X-ray matter interactions beyond the linear regime have been considered in a number of theoretical as well as experimental studies already for decades [8–10].

*Corresponding author. Email: simon.schreck@fysik.su.se

[1]Current address: Department of Physics, AlbaNova University Center, Stockholm University, SE-10691, Sweden.

This article was originally published with errors. This version has been corrected. Please see Corrigendum (http://dx.doi.org/10.1080/09500340.2015.1086128).

The early studies focused on spontaneous second-order nonlinear processes such as two-photon fluorescence in the hard X-ray regime. The employed theoretical models made use of the absence of resonances at very high X-ray energies, treating the electrons as a quasi-free plasma-like gas. More recently, second- and third-order resonant nonlinear processes in the soft and hard X-ray regime were modeled theoretically [11–14]. First experimental observations of two-photon absorption, amplified spontaneous emission and stimulated resonant X-ray scattering in gas phase and condensed systems have been reported [15–18]. The experimental observation of nonlinear X-ray processes has been facilitated by the advent of X-ray free-electron lasers (XFELs) [19–22], which provide femtosecond extreme ultraviolet (XUV) and X-ray pulses carrying 10^{12} to 10^{13} photons per pulse [23]. With this, the transfer of nonlinear concepts from the optical and infrared to the X-ray regime should become possible and enable nonlinear X-ray spectroscopies such as stimulated resonant X-ray scattering or X-ray four-wave mixing [11,24]. These nonlinear X-ray spectroscopies can benefit from enhanced signal levels as compared to their linear counter parts, which rely on spontaneous core-hole relaxation processes. In addition, they will provide significantly enhanced selectivity and sensitivity to the valence electronic structure and its dynamics.

A rigorous theoretical description of nonlinear X-ray-matter interactions is beyond the scope of this tutorial-type review, but the interested reader is referred to e.g. references [11–14]. Instead we will present a conceptual treatment of nonlinear X-ray processes with emphasis on stimulated resonant X-ray scattering and discuss the crucial experimental parameters. We apply an expression for the cross section of stimulated scattering derived originally by Lee and Albrecht in the 1980s [25] for the optical frequency regime. Patterson applied this formalism recently to the X-ray regime in his SLAC Technical Note [26]. The quantitative implementation provides a rough (order of magnitude) estimate for the required X-ray intensities to experimentally observe stimulated resonant X-ray scattering. Nevertheless, the scaling of this expression is valid for a wide range of photon energies encompassing the XUV, the soft and the hard X-ray regime. For the discussion we restrict ourselves to a fluence regime on dense samples, where saturation effects can be neglected since a sufficient number of scattering centers is always present. Based on this we analyze prospects and implications for spectroscopy, scattering, and imaging experiments at XFELs performed in the different XUV and X-ray photon energy regimes.

2. X-ray matter interactions and stimulated resonant X-ray scattering

We start with a discussion of basic aspects of X-ray matter interaction. For this, a description of the interaction of X-rays with matter as a scattering process is very instructive. In many cases, the scattering process can be separated into an excitation and a decay step. Figure 1 illustrates the different excitation and decay processes (which constitute the different scattering channels) in form of simplified single-electron energy level diagrams. In the excitation step an incident X-ray photon is absorbed by the scattering center (which we refer to as a molecule in the following). For appropriate photon energies, the absorption results in resonant excitation of a core-level electron into a formerly unoccupied valence level (Figure 1, box *A*). If the incident photon energy is sufficiently larger than the core-level binding energy (E_C), the molecule is ionized and the excited electron is transferred into the continuum (Figure 1, box *B*). The latter process is often denoted as nonresonant excitation. Resonant as well as nonresonant excitation result in a core-excited (core-ionized) molecule that has a vacancy in one of the core levels, a core hole. The core-excited state represents the intermediate state of the scattering process.

The intermediate core-excited state decays primarily by filling the core hole with an electron from an occupied valence level. Hereby, the excess energy can be released in the form of an X-ray photon (radiative decay) or it can be transferred to another valence electron, which is ejected from the molecule (nonradiative Auger decay), Figure 1. At the absence of a strong X-ray field the ratio between radiative and nonradiative decay depends strongly on the core-hole energy and core level (*K*-, *L*-, and *M*-shell hole). For core holes accessible by XUV and soft X-rays nonradiative decay dominates strongly, whereas for photon energies above ∼10 KeV radiative decay starts to dominate [27]. For resonant excitation the energy of the scattered photon or electron varies linearly with the incident photon energy, which is typical for a Raman-type scattering process. The radiative scattering channel is therefore referred to as "resonant X-ray Raman scattering", whereas the nonradiative scattering channel is referred to as "resonant Auger Raman scattering", Figure 1(*A*). For nonresonant excitation the energy of the emitted photon or electron is mostly independent of the excitation energy and its energy distribution reflects the valence electronic structure of the final state of the scattering process (which is in general not neutral, but a singly or doubly valence ionized state of the molecule). This is the basis of nonresonant X-ray emission and Auger electron spectroscopy. With increasing photon energy above the core-level binding energy the probability for resonantly exciting a core hole decreases and the photons will more likely scatter elastically. This scattering channel is mostly the basis for coherent X-ray scattering, diffraction, and imaging, Figure 1(*B*).

We now focus on resonant X-ray Raman scattering, i.e. the radiative decay channel after resonant excitation. In Figure 2 the different resonant scattering channels are illustrated again in the single-electron picture (box A), which illustrates solely electronic energy losses in the Raman scattering process. In box *B* of Figure 2 the same resonant

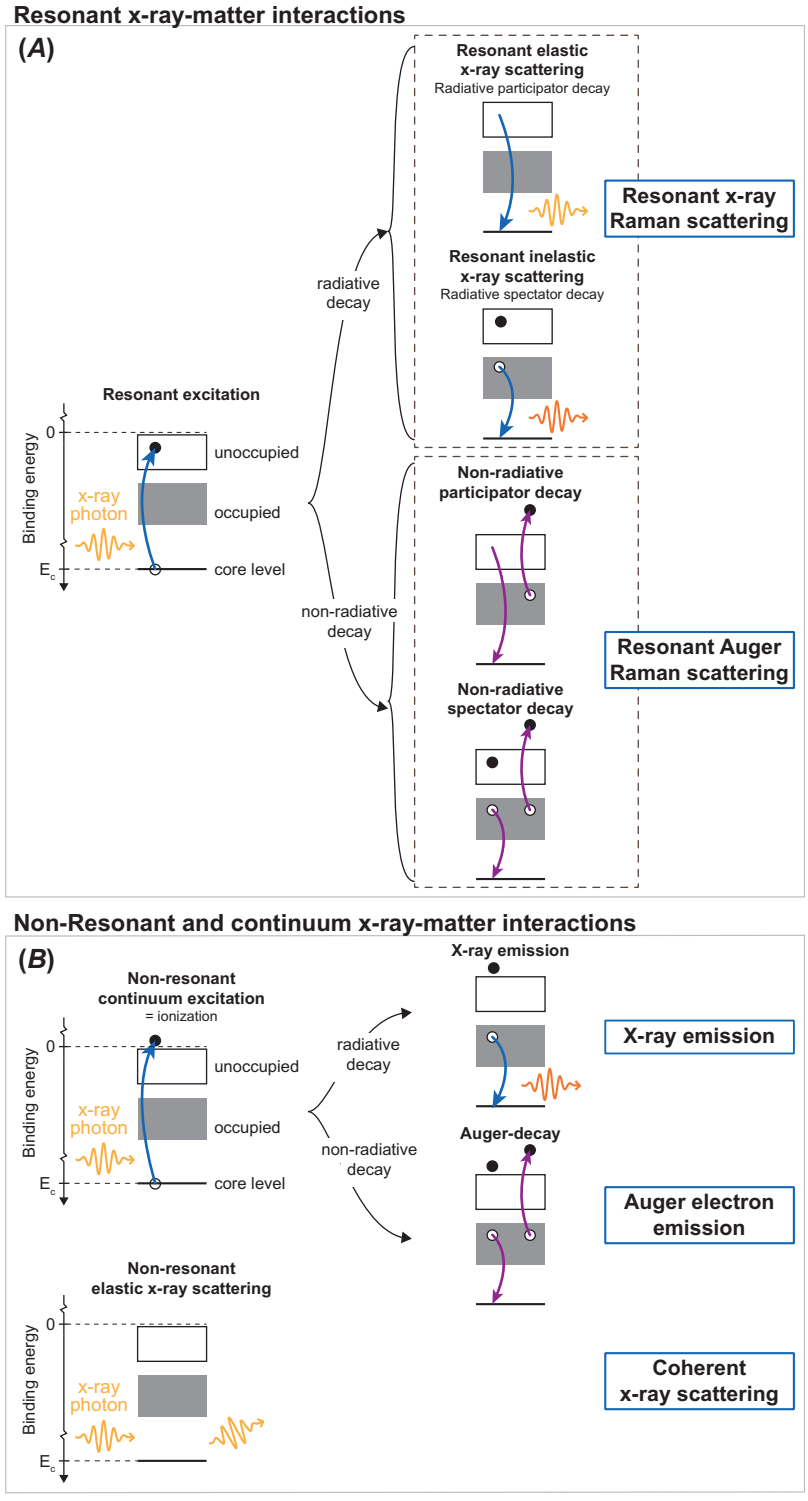

Figure 1. Fundamental X-ray-matter interactions illustrated in schematic single-electron energy level diagrams. The final electron configurations are shown for each process. See main text for discussion of the different processes. (The color version of this figure is included in the online version of the journal.)

scattering channels are illustrated in the strictly correct many-electron total energy picture. This picture describes the general case of resonant X-ray Raman scattering via a core-excited intermediate state, where the energy loss can correspond to an electronic, but also a vibrational, magnetic, or phonon excitation.

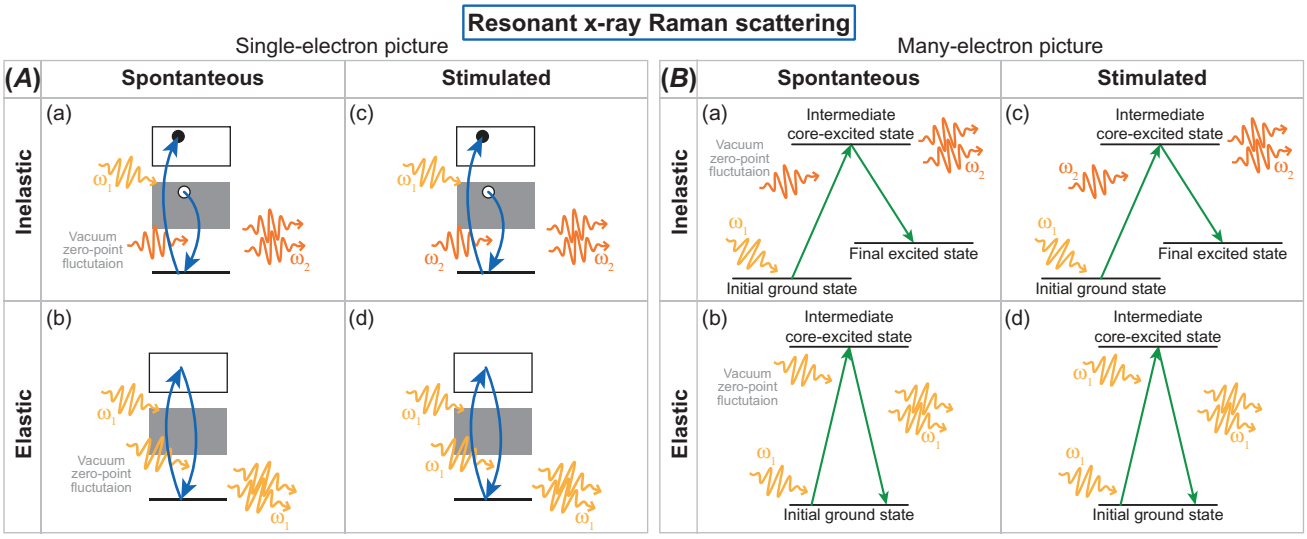

Figure 2. Resonant X-ray Raman scattering processes in the single-electron picture (*A*) as used in Figure 1 and in the many-electron total energy picture (*B*). In each picture, the spontaneous and stimulated as well as the inelastic and elastic scattering process are illustrated. (The color version of this figure is included in the online version of the journal.)

At the absence of a strong X-ray field the radiative decay of the intermediate core-excited state occurs spontaneously and is a result of vacuum zero-point fluctuations [28], Figure 2(a) and (b) in box *A* and *B*. However, the radiative decay can also be stimulated by an X-ray photon, which results in stimulated emission of a second X-ray photon with identical properties (energy, momentum, polarization) to the stimulating photon, Figure 2(c) and (d) in box *A* and *B*. The stimulated process competes with the spontaneous core-hole decay, where radiative as well as nonradiative spontaneous processes are important (remember that in the XUV and soft X-ray regime nonradiative core-hole decay is the dominating spontaneous process). For stimulated X-ray scattering to dominate more than one photon needs to be present around the scattering center during the typically femtosecond natural lifetime of the core-excited state (at least one photon to excite and one to stimulate). A comparison of typical intensities reveals that a sufficiently high photon flux is only available at XFELs: At a synchrotron a typical soft X-ray pulse of 100 ps duration carries $\sim 10^5$ photons [29,30]. This corresponds to one photon per femtosecond, i.e. during a typical core-hole lifetime only one photon is present in the whole irradiated volume of the sample. At an XFEL X-ray pulses of a few femtoseconds carry up to 10^{12} photons [23]. Hence, all these photons are present in the sample simultaneously during a typical core-hole lifetime and stimulated X-ray scattering becomes possible.

In general, the stimulating photons can be provided by an X-ray source, but they can also originate from spontaneous (or stimulated) X-ray emission processes at neighboring molecules. The latter situation results in amplification of the spontaneous emission signal and is denoted as amplified spontaneous emission (ASE). When the stimulating photon is provided directly by an X-ray source one should distinguish two situations: (1) The exciting and the stimulating photons come from the same X-ray pulse (impulsive stimulated scattering). (2) The exciting and the stimulating photons are provided by two different X-ray pulses ("classical" stimulated scattering). In any case, the stimulation process results in emission of a second X-ray photon with identical properties to the stimulating photon. Therefore, for impulsive stimulated scattering the stimulated signal propagates collinear with the incident beam into the forward direction. In ASE the angular distribution of the spontaneous emission signal, but also the spatial extent of the excited volume in the sample [16] determine the direction of maximized stimulated signal. In the two-pulse scheme, the direction of the (second) stimulating X-ray pulse determines the direction of the stimulated signal and allows for separate detection of the stimulated signal.

3. Cross section estimate for stimulated resonant X-ray scattering

To estimate the required X-ray photon flux to perform a stimulated X-ray scattering experiment at an XFEL we employ a formalism presented by Lee and Albrecht [25]. These authors derived an expression for the cross section of stimulated scattering at optical frequencies in the 1980s. Following an idea put forward by B. Patterson in his SLAC Technical Note [26] we derive an expression for the cross section of stimulated X-ray scattering, which is directly related to the spontaneous emission and Auger decay cross sections.

Lee and Albrecht [25] used a density matrix formalism and considered the work performed by the electromagnetic field in a medium to derive the cross section for stimulated scattering. Using the mks-units system (i.e. SI units) the stimulation cross section from Lee and Albrecht [25] reads

$$\frac{\mathrm{d}^2\sigma_{\mathrm{stim}}}{\mathrm{d}\Omega\mathrm{d}\omega_2} = \frac{\hbar\,\omega_1\omega_2}{2\,\epsilon_0 c^2}\,F(\omega_2)\,\frac{\mathrm{Im}(\chi^{(3)})}{\rho}. \tag{1}$$

This double differential cross section describes stimulated scattering of an incident photon at frequency ω_1 into the solid angle $\mathrm{d}\Omega$ and frequency interval $[\omega_2, \omega_2 + d\omega_2]$ under presence of an (intense) stimulating photon field at frequency ω_2 (see Figure 2(c)). $F(\omega_2)$ is the spectral photon flux (photons per area, time, and frequency interval) of the stimulating photon field. ρ is the number density of scattering centers in the medium. The third-order nonlinear susceptibility $\chi^{(3)}$ is a material property and describes the nonlinear response of the polarization in the medium upon the applied fields at frequencies ω_1 and ω_2. In general $\chi^{(3)}$ is a fourth-rank tensor. For the stimulated scattering process that we discuss, the frequency dependence is $\chi^{(3)} = \chi^{(3)}(\omega_2 = \omega_2 + \omega_1 - \omega_1)$ [1].

Spontaneous X-ray emission can be treated conceptually in the same way as stimulated X-ray scattering, where the so-called vacuum zero-point field is regarded as the stimulating field for spontaneous emission (Section 2 and Figure 2(a) and (b)). Hence, the cross section for spontaneous emission can be derived from Equation (1) by inserting the vacuum zero-point photon flux $F_{\mathrm{ZP}}(\omega_2)$ for $F(\omega_2)$ [25]. An estimate for $F_{\mathrm{ZP}}(\omega_2)$ can be obtained from Plancks radiation law for the black body spectrum including the zero-point energy [31–33]

$$F_{\mathrm{BB}}(\omega, T) = \frac{\omega^2}{2\pi^2 c^2}\left(\frac{1}{\mathrm{e}^{\frac{\hbar\omega}{kT}} - 1} + \frac{1}{2}\right). \tag{2}$$

Equation (2) gives the black body photon flux (photons per area, time, and frequency interval) per unit solid angle as a function of temperature T and photon frequency ω. In vacuum and at temperature $T = 0\,\mathrm{K}$ the zero-point photon flux remains

$$F_{\mathrm{ZP}}(\omega) = \frac{\omega^2}{4\pi^2 c^2}. \tag{3}$$

Inserting (3) into (1) the cross section for spontaneous emission follows

$$\frac{\mathrm{d}^2\sigma_{\mathrm{spon}}}{\mathrm{d}\Omega\mathrm{d}\omega_2} = \frac{\hbar\,\omega_1\omega_2^3}{8\pi^2\epsilon_0 c^4}\,\frac{\mathrm{Im}(\chi^{(3)})}{\rho}. \tag{4}$$

To check the validity of the zero-point approach and the resulting expression for the spontaneous emission cross Section (4) we use a value for the third-order nonlinear susceptibility of $\mathrm{Im}(\chi^{(3)}) = 10^{-21}\,\mathrm{m}^2/\mathrm{V}^2$, which is the order of magnitude estimated in recent publications [11,24,26] for resonant carbon K-shell scattering at ~277 eV (Note that the exact value given for $\chi^{(3)}$ varies by one to two orders of magnitude between the publications). Using the atomic density of amorphous carbon of $\rho \approx 10^{-29}\,\mathrm{m}^{-3}$ and the carbon 1s line width (0.07 eV [27]) a spontaneous emission cross section of $\mathrm{d}\sigma_{\mathrm{spon}}/\mathrm{d}\Omega = 3.1 \times 10^{-25}\,\mathrm{m}^2$ follows from Equation (4). This value compares reasonably well (noting the rough estimate for $\chi^{(3)}$) with the spontaneous emission cross section obtained from the tabulated total carbon 1s absorption cross section $\sigma_{\mathrm{abs}} = 1.1 \times 10^{-22}\,\mathrm{m}^2$ [34], the carbon 1 s fluoresence yield $w_{\mathrm{fy}} = 3 \times 10^{-3}$ [27] and assuming isotropic spontaneous emission into 4π: $\mathrm{d}\sigma_{\mathrm{spon}}/\mathrm{d}\Omega = \sigma_{\mathrm{abs}}\,w_{\mathrm{fy}}/(4\pi) = 2.6 \times 10^{-26}\,\mathrm{m}^2$.

Combining Equations (4) and (1) we obtain a relation between the cross section for stimulated and spontaneous emission

$$\frac{\mathrm{d}^2\sigma_{\mathrm{stim}}}{\mathrm{d}\Omega\mathrm{d}\omega_2} = \frac{4\pi^2 c^2}{w_2^2}\,\frac{\mathrm{d}^2\sigma_{\mathrm{spon}}}{\mathrm{d}\Omega\mathrm{d}\omega_2}\,F(\omega_2). \tag{5}$$

Equation (5) is independent of any material constants and in particular independent of the nonlinear susceptibility $\chi^{(3)}$. Hence, (5) provides an estimate of the stimulated X-ray scattering cross section with no need for an (in general very rough) estimate for $\chi^{(3)}$ in the X-ray regime. In addition, (5) allows a direct comparison of the cross sections for stimulated scattering, spontaneous emission as well as Auger decay (the ratio of spontaneous emission and Auger decay is given by tabulated fluorescence yields [27]).

When the sample is dense enough as compared to the photon flux, such that saturation effects can be neglected and a sufficient number of unexcited molecules is always present, we can compare the cross sections for scattering via spontaneous X-ray emission ($\mathrm{d}\sigma_{\mathrm{spon}}/\mathrm{d}\Omega$), nonradiative Auger decay ($\mathrm{d}\sigma_{\mathrm{Auger}}/\mathrm{d}\Omega$) and stimulated X-ray scattering ($\mathrm{d}\sigma_{\mathrm{stim}}/\mathrm{d}\Omega$). In this case, we note that the total scattering cross section

$$\sigma_{\mathrm{tot}} = \sigma_{\mathrm{spon}} + \sigma_{\mathrm{Auger}} + \sigma_{\mathrm{stim}} \tag{6}$$

is a constant for a given photon energy. However, in the high intensity limit of the range considered in this work, the assumption of negligible saturation may be violated and effects like Rabi oscillations [31,35,36] may become important. This would effectively decrease the absorption cross section and with this also σ_{tot}. In Equation (6) we dropped the $\mathrm{d}\Omega$ for readability and will do so in the following. However, it should be remembered that all cross sections refer to scattering into the solid angle $\mathrm{d}\Omega$ integrated over the natural line width of the respective core level.

The total scattering cross section σ_{tot} can be estimated by the absorption cross section σ_{abs} divided by 4π to account for assumed isotropic scattering. Sizable stimulated scattering will decrease the relative contributions of spontaneous emission and Auger decay to the total scattering cross section. In addition, stimulated scattering will focus the scattering signal into the propagation direction of the stimulating field. This yields to strongly anisotropic stimulated scattering. We neglect the focusing effect of stimulated

scattering here for the quantitative estimate, but discuss its qualitative implications in Section 5.

The ratio between spontaneous emission and Auger decay is independent of the magnitude of stimulated scattering and is determined by the fluorescence yield w_{fy} via

$$\sigma_{\mathrm{Auger}} = \sigma_{\mathrm{spon}} \frac{1 - w_{\mathrm{fy}}}{w_{\mathrm{fy}}}. \tag{7}$$

Inserting Equations (5) and (7) into Equation (6) links the spontaneous emission cross section to the total scattering cross section:

$$\sigma_{\mathrm{tot}} = \sigma_{\mathrm{spon}} \left(1 + \frac{1 - w_{\mathrm{fy}}}{w_{\mathrm{fy}}} + \frac{4\pi^2 c^2}{w_2^2} F(\omega_2) \right). \tag{8}$$

Equations (5), (7) and (8) allow us now to compare the cross sections for scattering via spontaneous and stimulated X-ray emission as well as Auger decay. We do so for the case of resonant K-shell scattering ($\omega_1 = \omega_2 = \omega_{\mathrm{res}}$) and use tabulated values [34] for the resonant K-shell absorption cross section σ_{abs} between lithium (50 eV) and molybdenum (20 keV) and tabulated [27,37] fluorescence yields. With this we calculate σ_{stim}, σ_{spon} and σ_{Auger} as a function of resonance photon energy and stimulating photon flux $F(\omega_2)$. For the stimulating photon flux we assumed XFEL pulses of 10 fs duration, 0.5% photon energy bandwidth, a focal size of $50 \times 50\,\mu\mathrm{m}^2$ and 10^{10} to 10^{15} photons per pulse. This covers the intensity regime currently available at XFELs as well as a regime exceeding the capabilities of XFELs at XUV, soft and hard X-ray photon energies. It should be noted that the relevant intensity ($F(\omega_2)$) is the spectral photon flux, i.e. the number of photons per time, area, and spectral bandwidth. Hence, a lower photon number per pulse can be compensated by tighter focusing of the X-ray beam or in principle also by a shorter pulse length or smaller energy bandwidth. However, we use for the following discussion the number of photons per pulse (implicitly assuming the above pulse parameters), since this is an *easy to grasp* parameter. Furthermore we note that, though the calculation is performed for K-shell scattering here, the presented results are also a good estimate for other shells. Since the core-hole lifetimes and level width are on the same order of magnitude for e.g. K- and L-shells at the same resonance photon energy, the cross sections scale mainly with the resonance photon energy.

In Figure 3, top panel, we present a three-dimensional surface plot of σ_{stim}, σ_{spon} and σ_{Auger} as a function of resonance photon energy and stimulating photon flux $F(\omega_2)$. Already here general trends become apparent: the stimulation cross section increases with increasing stimulating photon flux and decreases with increasing resonance photon energy. Furthermore, independently of the stimulating photon flux, the Auger decay cross section dominates over the spontaneous emission cross section in the XUV and soft X-ray photon energy range. At around 10 keV resonance photon energy spontaneous emission starts to dominate over Auger decay.

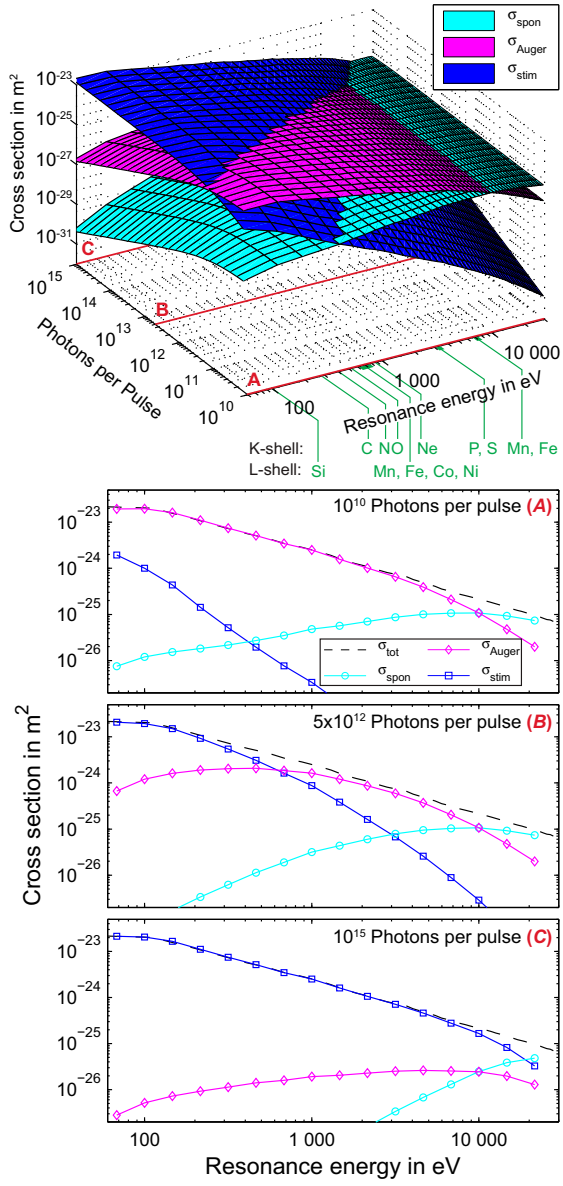

Figure 3. Competition between scattering via stimulated and spontaneous radiative decay as well as via nonradiative Auger decay. The respective cross sections estimated from the model described in the main text are plotted as a function of the stimulating photon flux and resonance photon energy. The stimulating photon flux is given in photons per pulse assuming 10 fs pulse duration, 0.5% photon energy bandwidth and a focal spot size of $50 \times 50\,\mu\mathrm{m}^2$. Red lines indicate the cut positions displayed in panel (*A*)–(*C*). K- and L-shell resonance energies for selected elements are indicated and the respective cuts are displayed in Figure 4. (The color version of this figure is included in the online version of the journal.)

For a more quantitative analysis we present cuts though the three-dimensional data-set at fixed stimulating photon flux in Figure 3, panel (*A*)–(*C*). Cuts at characteristic reso-

nance photon energies are shown in Figure 4. Here, the stimulating photon flux $F(\omega_2)$ is also given in W/cm^2 (upper x-axes) in addition to the number of photons per pulse (lower x-axes). In the cut plots we also include the total scattering cross section σ_{tot}. The general trend of smaller σ_{tot} for higher resonance photon energy is directly visible in Figures 3 and 4 and obviously independent of the stimulating photon flux $F(\omega_2)$. Another general trend is the lower stimulation cross section relative to the spontaneous emission cross sections with increasing resonance photon energy.

However, for the low-intensity regime ($\sim 10^{10}$ photons per pulse) the spontaneous emission and Auger cross sections dominate over the stimulation cross section also at the lowest XUV resonance energies. At around 100 eV resonance energy (Figure 4(*A*)), which corresponds to e.g. the silicon L-edge, where ASE has been recently observed [16], around 5×10^{11} photons per pulse ($\sim 10^{13}$ W/cm^2) are required for the stimulation cross section to exceed the Auger cross section.

The soft X-ray regime covers the K-edges of elements like carbon, nitrogen, and oxygen (Figure 4(*B*)) that are intensively studied by X-ray spectroscopy and scattering techniques due to their relevance in nature [38–40], catalysis [41,42] or biological systems [43,44] as well as the L-edges of elements such as manganese and iron (Figure 4(*C*)) that play a central role in photosynthesis [45] or other photochemical reactions [46]. At the neon K-edge at around 870 eV photon energy (Figure 4(*C*)) ASE had been realized experimentally for the first time in the gas phase [15]. At these resonance energies intensities of 5×10^{12} to 10^{13} photons per pulse (~ 1 to 5×10^{15} W/cm^2) are required for the stimulation cross section to exceed the Auger cross section.

At photon energies of $\sim$2200 eV corresponding to the phosphorous or sulfur K-edges in the tender X-ray regime (Figure 4(*D*)), where crystallographic techniques such as single- or multiwavelength anomalous diffraction (SAD or MAD) are routinely applied [47] around 5×10^{13} photons per pulse ($\sim 5 \times 10^{16}$ W/cm^2) are required for the stimulation cross section to exceed the Auger cross section.

The threshold intensities estimated so far for the XUV, soft and tender X-ray regime are within the capabilities of current XFELs in this photon energy range. Hence stimulated X-ray scattering should be experimentally feasible at these photon energies and first pioneering experiments have confirmed this conclusion [15–17].

The hard X-ray regime comprises, among others, the K-edges of manganese, and iron at around 7 keV resonance energy (Figure 4(*E*)) that are equally relevant for photosynthesis and photochemistry [48,49] than the corresponding L-edges. Furthermore, coherent X-ray scattering and imaging experiments are typically performed at these photon energies [50]. In this regime, already quite high intensities of around 10^{14} photons per pulse ($\sim 5 \times 10^{17}$ W/cm^2) are necessary for stimulated scattering to dominate over the spontaneous scattering channels. At even higher photon energies of $\sim$15 keV (Figure 4(*F*)), which are required to achieve atomic resolution on the angstrom length scale in scattering and imaging experiments intensities of 5×10^{14} photons per pulse ($\sim 5 \times 10^{18}$ W/cm^2) are required for stimulated scattering. These intensities are beyond the capabilities of current XFELs in the hard X-ray regime.

4. Implications for resonant X-ray spectroscopy at free-electron lasers

The cross section estimate from Section 3 implies that stimulated resonant X-ray scattering should be experimentally observable with intensities achievable at current XFEL light sources in the XUV and soft X-ray photon energy range. For hard X-ray photon energies on the other hand X-ray intensities that are beyond the capabilities of current XFEL sources are needed for stimulated X-ray scattering to dominate over spontaneous X-ray emission. First pioneering experiments in the XUV and soft X-ray regime verify this conclusion: at the Ne K-edge ($\sim$860 eV) ASE as well as stimulated X-ray scattering have been observed in the gas phase [15,17]. In the condensed phase ASE was observed at the Si L-edge ($\sim$100 eV) in crystalline silicon [16]. These are first steps that pave the way for more advanced and complex nonlinear spectroscopic schemes to be transferred from the optical and infrared into the XUV and soft X-ray regime.

Establishing stimulated X-ray scattering for resonant soft X-ray spectroscopies such as resonant X-ray Raman scattering will considerably enhance the usually very low signal levels for these highly selective probes of the valence electronic structure. Stimulated X-ray emission in the XUV and soft X-ray regime suppresses the dominating Auger decay, which at the same time reduces electronic sample damage and in turn enables higher incident X-ray intensities to be used. This is true for ASE as well as impulsive stimulated X-ray scattering, which are possible with a single intense XUV or soft X-ray XFEL pulse. However, the separation of the stimulated signal from the direct beam might be problematic in single pulse experiments (see also discussion in Section 5). The two-pulse schemes, where a first X-ray pulse resonantly excites a specific core-excited state and a second X-ray pulse resonantly stimulates a specific decay transition of this core-excited state can overcome the detection problem and will further enhance the selectivity of resonant X-ray spectroscopies. Including a third X-ray pulse that resonantly excites a core-excited state at a different atomic center is a very intriguing possibility to enable X-ray four-wave mixing experiments. Such experimental schemes should allow for probing valence electron correlations between different atomic sites within large molecules or correlated materials [11].

Stimulated X-ray scattering should furthermore provide an elegant way of controlling the scattering time in resonant X-ray Raman scattering experiments. Using ultrashort

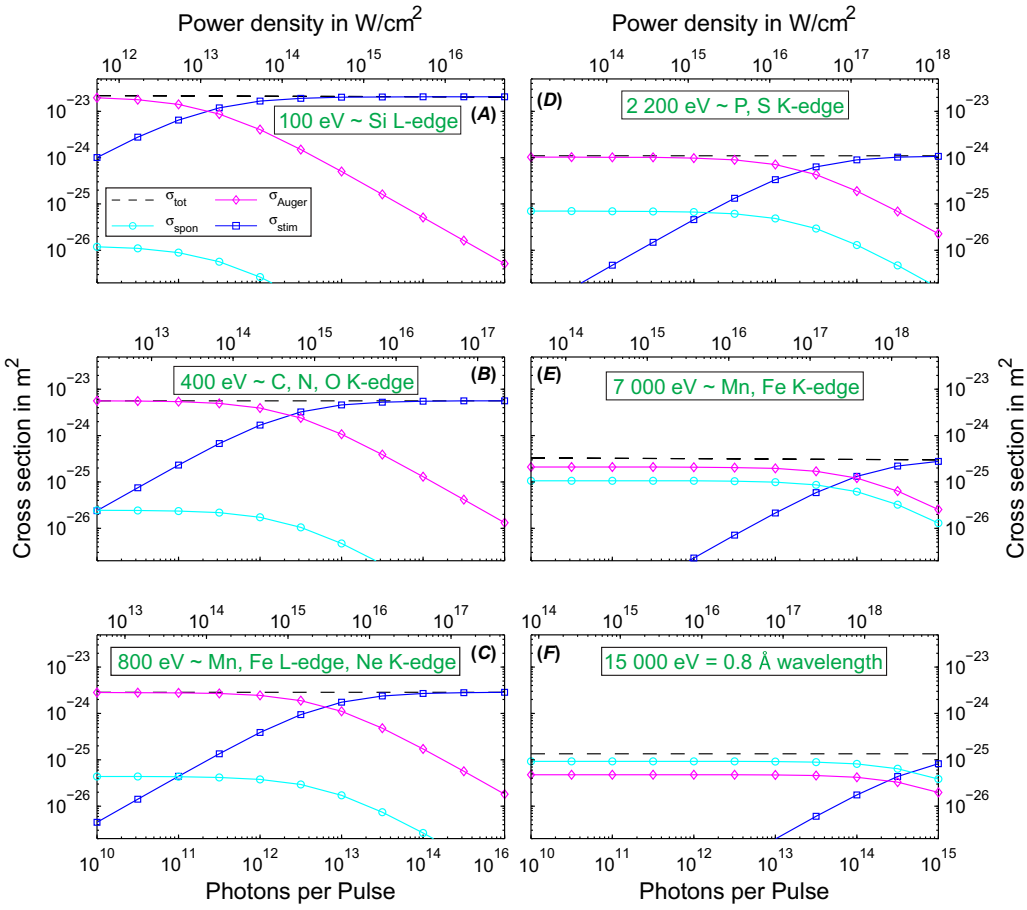

Figure 4. Cuts through the three-dimensional data-set at fixed resonance photon energies corresponding to relevant *K*- and *L*-shell scattering resonances. The lower *x*-axes give the intensity in photons per pulse and are identical in each panel (tickmarks are given only in panel (*C*) and (*F*)). The upper *x*-axes give the intensity in $\mathrm{W/cm^2}$ and are different for each panel due to different resonance photon energies. (The color version of this figure is included in the online version of the journal.)

pulses of one femtosecond and less (significantly shorter that the natural core-hole lifetime), the decay of core-excited states can be stimulated at any time within the natural core-hole lifetime. This will allow a detailed study of dynamic effects induced by core-level excitations. Furthermore the creation of valence excitations at selected atomic centers can be timed with an accuracy well below the natural core-hole lifetime.

Any of these multi-pulse nonlinear X-ray spectroscopic schemes places high demands on the X-ray pulse structures. They require independently tunable X-ray pulses covering a difference in photon energy of at least several electron volts and pulse durations as well as interpulse delays of few femtoseconds and less. In addition, the incident angles of the individual pulses should be variable to separately detect their signals as well as to study the momentum transfer in crystalline structures.

To meet the high demands on the X-ray pulse structures the current instrumental developments at XFEL facilities that include, among others, seeding schemes [22,51] to reduce the shot-to-shot fluctuations of the spectral and temporal pulse structure as well as split and delay techniques for XFEL pulses [52,53] need to be pushed forward. At the same time a parallel development that might soon be able to deliver pulse structures and intensities to perform nonlinear X-ray spectroscopies are laboratory-based high harmonic sources [54,55]. These sources currently undergo rapid developments and are already able to produce attosecond soft X-ray pulses [56,57].

5. Implications for coherent diffraction and imaging at free-electron lasers

Stimulated X-ray scattering collects the scattering intensity into a narrow cone pointing into the direction of the stimulating X-ray beam and suppresses the scattering signal into other directions. Impulsive stimulated scattering will therefore collect the scattering signal into the forward direction, where it can be detected only after strong attenuation

and is in general hard to distinguish from the intensity of the direct beam. This is a fundamental problem for any kind of scattering experiment, including resonant X-ray Raman scattering or X-ray emission spectroscopy as well as coherent diffraction and imaging.

For resonant X-ray Raman scattering experiments, where the energy distribution of the scattered X-rays is of interest, a two-pulse scheme with the stimulating X-ray beam under a different incident angle than the exciting X-ray beam will solve this problem (Section 4). However, for coherent diffraction and imaging experiments, where the angular distribution of the scattering signal (scattering pattern) is of interest the focusing effect of stimulated scattering remains a conceptual problem that may become severe toward high XFEL fluences.

On the other hand, coherent diffraction and imaging experiments are typically performed at photon energies of several keV (corresponding to a few Å wavelength) to ultimately achieve atomic resolution. As we have seen in Section 3, the stimulation cross section drops quickly with increasing photon energy when compared to the cross sections for spontaneous decay processes. In fact, for the hard X-ray regime sizable stimulation will set in only at very high incident X-ray intensities. At 15 keV only for intensities of about 5×10^{14} photons per pulse and the pulse parameter used in Section 3, which corresponds to $\sim 5 \times 10^{18}\,\mathrm{W/cm^2}$ (see Section 3 and Figures 3 and 4) the cross sections for resonant stimulated scattering and spontaneous core-hole decay become comparable. In addition, this threshold estimate applies for resonant stimulated scattering only. Coherent diffraction and imaging are based on nonresonant scattering of hard X-rays at light elements with core-level binding energies far below the X-ray photon energy. Nonresonant scattering cross sections are typically from one to two orders of magnitude lower than resonant scattering cross sections [58]. Hence, the threshold for nonresonant stimulated scattering should also be at one to two orders of magnitude higher incident intensities as compared to the threshold for resonant stimulated scattering.

In conclusion, for currently available XFEL intensities as well as for most of the intensities aimed for in future single molecule imaging experiments in the hard X-ray regime [59] there should be no significant effect from stimulated scattering.

A widely applied technique to overcome the phase problem in crystallography is multiwavelength anomalous diffraction (MAD) [47], which is based on resonant scattering at e.g. the phosphorus and sulfur K-edges (around 2.1 and 2.5 keV). At these rather low resonance energies, stimulation may be able to dominate at currently available XFEL intensities. However, the concentration of scattering centers is typically very low for these techniques, which may weight out the comparable high stimulation cross section. Also MAD should therefore not be affected by focusing due to stimulated scattering.

6. Conclusions and summary

We presented a conceptual treatment of nonlinear X-ray-matter interactions with an emphasize on stimulated resonant X-ray scattering. The quantitative estimate for the stimulated scattering cross section in the X-ray regime shows that stimulated resonant X-ray scattering should be experimentally observable with intensities achievable at current XFEL light sources in the XUV and soft X-ray photon energy range. First pioneering experiments verify this conclusion and pave the way for more advanced and complex nonlinear spectroscopic schemes to be transferred from the optical and infrared into the XUV and soft X-ray regime. For higher X-ray photon energies of several keV intensities that are beyond the capabilities of current XFEL light sources are needed for sizable stimulated X-ray scattering. The low-stimulation cross section in the hard X-ray regime is beneficial for coherent diffraction and imaging experiments, which are typically performed at several keV photon energies (corresponding to a few Å wavelengths). The focusing effect of stimulated X-ray scattering would in these experiments collect the scattering signal into the direct beam and result in an unwanted decrease in the scattered intensity signal.

Disclosure statement

No potential conflict of interest was reported by the authors.

Funding

Funding has been provided by the Helmholtz Zentrum Berlin, by the BMBF Röntgen Angström Cluster project [05K12IP2], the Helmholtz Virtual Institute "Dynamic Pathways in Multidimensional Landscapes" and the Volkswagen Stiftung.

References

[1] Boyd, R.W. *Nonlinear Optics*; Elsevier, Academic Press, Amsterdam, 2008.
[2] Franken, P.A.; Hill, A.E.; Peters, C.W.; Weinreich, G. *Phys. Rev. Lett.* **1961,** *7,* 118–119.
[3] Herzberg, G. *Molecular Spectra and Molecular Structure II: Infrared and Raman of Polyatomic Molecules*; Schrader, B., Ed.; D. Van Nostrand Company Inc., Princeton, NJ, 1950.
[4] Bougeard, D.; Buback, M.; Cao, A.; Gerwert, K.; Heise, H.M.; Hoffmann, G.G.; Jordanov, B.; Kiefer, W.; Korte, E.H.; Kuzmany, H.; Leipertz, A.; Lentz, E.; Liquier, J.; Roseler, A.; Schnockel, H.; Schrader, B.; Schrotter, H.W.; Spiekermann, M.; Taillandier, E.; Willner, H. *Infrared and Raman Spectroscopy: Methods and Applications*; VCH Verlagsgesellschaft mbH: Weinheim, 1995.
[5] Bergh, M.; Tîmneanu, N.; Van Der Spoel, D. *Phys. Rev. E - Stat. Nonlinear Soft Matter Phys.* **2004,** *70,* 1–7.
[6] Bergh, M.; Tîmneanu, N.; Hau-Riege, S.P.; Scott, H.A. *Phys. Rev. E - Stat. Nonlinear Soft Matter Phys.* **2008,** *77,* 1–8.
[7] Schreck, S.; Beye, M.; Sellberg, J.A.; McQueen, T.; Laksmono, H.; Kennedy, B.; Eckert, S.; Schlesinger, D.; Nordlund, D.; Ogasawara, H.; Sierra, R.G.; Segtnan, V.H.; Kubicek, K.; Schlotter, W.F.; Dakovski, G.L.; Moeller, S.P.;

Bergmann, U.; Techert, S.; Pettersson, L.G.M.; Wernet, P.; Bogan, M.J.; Harada, Y.; Nilsson, A.; Föhlisch, A. *Phys. Rev. Lett*. **2014,** *113,* 153002-1–153002-6.
[8] Freund, I.; Levine, B.F. *Phys. Rev. Lett*. **1969,** *23,* 854–857.
[9] Eisenberger, P.; McCall, S.L. *Phys. Rev. Lett*. **1971,** *26,* 684–688.
[10] Freund, I. *Opt. Commun*. **1972,** *6,* 421–423.
[11] Tanaka, S.; Mukamel, S. *Phys. Rev. Lett*. **2002,** *89,* 043001-1–043001-4.
[12] Rohringer, N.; Santra, R. *Phys. Rev. A* **2007,** *76,* 033416-1–033416-10.
[13] Sun, Y.P.; Rinkevicius, Z.; Wang, C.K.; Carniato, S.; Simon, M.; Taïeb, R.; Gel'Mukhanov, F. *Phys. Rev. A – Atomic Mol. Opt. Phys*. **2010,** *82,* 1–8.
[14] Weninger, C.; Rohringer, N. *Phys. Rev. A* **2013,** *88,* 053421-1–053421-8.
[15] Rohringer, N.; Ryan, D.; London, R.A.; Purvis, M.; Albert, F.; Dunn, J.; Bozek, J.D.; Bostedt, C.; Graf, A.; Hill, R.; Hau-Riege, S.P.; Rocca, J.J. *Nature* **2012,** *481,* 488–491.
[16] Beye, M.; Schreck, S.; Sorgenfrei, F.; Trabant, C.; Pontius, N.; Schüßler-Langeheine, C.; Wurth, W.; Föhlisch, A. *Nature* **2013,** *501,* 191–194.
[17] Weninger, C.; Purvis, M.; Ryan, D.; London, R.; Bozek, J.; Bostedt, C.; Graf, A.; Brown, G.; Rocca, J.J.; Rohringer, N. *Phys. Rev. Lett*. **2013,** *111,* 233902-1–233902-5.
[18] Tamasaku, K.; Shigemasa, E.; Inubushi, Y.; Katayama, T.; Sawada, K.; Yumoto, H.; Ohashi, H.; Mimura, H.; Yabashi, M.; Yamauchi, K.; Ishikawa, T. *Nat. Photonics* **2014,** *8,* 313–316.
[19] Ackermann, W.; Asova, G.; Ayvazyan, V.; Azima, A.; Baboi, N.; Bähr, J.; Balandin, V.; Beutner, B.; Brandt, A.; Bolzmann, A.; Brinkmann, R.; Brovko, O.I.; Castellano, M.; Castro, P.; Catani, L.; Chiadroni, E.; Choroba, S.; Cianchi, A.; Costello, J.T.; Cubaynes, D.; Dardis, J.; Decking, W.; Delsim-Hashemi, H.; Delserieys, A.; Di Pirro, G.; Dohlus, M.; Düsterer, S.; Eckhardt, A.; Edwards, H.T.; Faatz, B.; Feldhaus, J.; Flöttmann, K.; Frisch, J.; Fröhlich, L.; Garvey, T.; Gensch, U.; Gerth, C.; Görler, M.; Golubeva, N.; Grabosch, H.J.; Grecki, M.; Grimm, O.; Hacker, K.; Hahn, U.; Han, J.H.; Honkavaara, K.; Hott, T.; Hüning, M.; Ivanisenko, Y.; Jaeschke, E.; Jalmuzna, W.; Jezynski, T.; Kammering, R.; Katalev, V.; Kavanagh, K.; Kennedy, E.T.; Khodyachykh, S.; Klose, K.; Kocharyan, V.; Körfer, M.; Kollewe, M.; Koprek, W.; Korepanov, S.; Kostin, D.; Krassilnikov, M.; Kube, G.; Kuhlmann, M.; Lewis, C.L.S.; Lilje, L.; Limberg, T.; Lipka, D.; Löhl, F.; Luna, H.; Luong, M.; Martins, M.; Meyer, M.; Michelato, P.; Miltchev, V.; Möller, W.D.; Monaco, L.; Müller, W.F.O.; Napieralski, O.; Napoly, O.; Nicolosi, P.; Nölle, D.; Nuñez, T.; Oppelt, A.; Pagani, C.; Paparella, R.; Pchalek, N.; Pedregosa-Gutierrez, J.; Petersen, B.; Petrosyan, B.; Petrosyan, G.; Petrosyan, L.; Pflüger, J.; Plönjes, E.; Poletto, L.; Pozniak, K.; Prat, E.; Proch, D.; Pucyk, P.; Radcliffe, P.; Redlin, H.; Rehlich, K.; Richter, M.; Roehrs, M.; Roensch, J.; Romaniuk, R.; Ross, M.; Rossbach, J.; Rybnikov, V.; Sachwitz, M.; Saldin, E.L.; Sandner, W.; Schlarb, H.; Schmidt, B.; Schmitz, M.; Schmüser, P.; Schneider, J.R.; Schneidmiller, E.A.; Schnepp, S.; Schreiber, S.; Seidel, M.; Sertore, D.; Shabunov, A.V.; Simon, C.; Simrock, S.; Sombrowski, E.; Sorokin, A.A.; Spanknebel, P.; Spesyvtsev, R.; Staykov, L.; Steffen, B.; Stephan, F.; Stulle, F.; Thom, H.; Tiedtke, K.; Tischer, M.; Toleikis, S.; Treusch, R.; Trines, D.; Tsakov, I.; Vogel, E.; Weiland, T.; Weise, H.; Wellhöfer, M.; Wendt, M.; Will, I.; Winter, A.; Wittenburg, K.; Wurth, W.; Yeates, P.; Yurkov, M.V.; Zagorodnov, I.; Zapfe, K. *Nat. Photonics* **2007,** *1,* 336–342.
[20] Emma, P.; Akre, R.; Arthur, J.; Bionta, R.; Bostedt, C.; Bozek, J.; Brachmann, A.; Bucksbaum, P.; Coffee, R.; Decker, F.J.; Ding, Y.; Dowell, D.; Edstrom, S.; Fisher, A.; Frisch, J.; Gilevich, S.; Hastings, J.; Hays, G.; Hering, P.; Huang, Z.; Iverson, R.; Loos, H.; Messerschmidt, M.; Miahnahri, A.; Moeller, S.; Nuhn, H.D.; Pile, G.; Ratner, D.; Rzepiela, J.; Schultz, D.; Smith, T.; Stefan, P.; Tompkins, H.; Turner, J.; Welch, J.; White, W.; Wu, J.; Yocky, G.; Galayda, J. *Nat. Photonics* **2010,** *4,* 641–647.
[21] Ishikawa, T.; Aoyagi, H.; Asaka, T.; Asano, Y.; Azumi, N.; Bizen, T.; Ego, H.; Fukami, K.; Fukui, T.; Furukawa, Y.; Goto, S.; Hanaki, H.; Hara, T.; Hasegawa, T.; Hatsui, T.; Higashiya, A.; Hirono, T.; Hosoda, N.; Ishii, M.; Inagaki, T.; Inubushi, Y.; Itoga, T.; Joti, Y.; Kago, M.; Kameshima, T.; Kimura, H.; Kirihara, Y.; Kiyomichi, A.; Kobayashi, T.; Kondo, C.; Kudo, T.; Maesaka, H.; Maréchal, X.M.; Masuda, T.; Matsubara, S.; Matsumoto, T.; Matsushita, T.; Matsui, S.; Nagasono, M.; Nariyama, N.; Ohashi, H.; Ohata, T.; Ohshima, T.; Ono, S.; Otake, Y.; Saji, C.; Sakurai, T.; Sato, T.; Sawada, K.; Seike, T.; Shirasawa, K.; Sugimoto, T.; Suzuki, S.; Takahashi, S.; Takebe, H.; Takeshita, K.; Tamasaku, K.; Tanaka, H.; Tanaka, R.; Tanaka, T.; Togashi, T.; Togawa, K.; Tokuhisa, A.; Tomizawa, H.; Tono, K.; Wu, S.; Yabashi, M.; Yamaga, M.; Yamashita, A.; Yanagida, K.; Zhang, C.; Shintake, T.; Kitamura, H.; Kumagai, N. *Nat. Photonics* **2012,** *6,* 540–544.
[22] Allaria, E.; Appio, R.; Badano, L.; Barletta, W.; Bassanese, S.; Biedron, S.; Borga, A.; Busetto, E.; Castronovo, D.; Cinquegrana, P.; Cleva, S.; Cocco, D.; Cornacchia, M.; Craievich, P.; Cudin, I.; D'Auria, G. Dal Forno, M.; Danailov, M.; De Monte, R.; De Ninno, G.; Delgiusto, P.; Demidovich, A.; Di Mitri, S.; Diviacco, B.; Fabris, A.; Fabris, R.; Fawley, W.; Ferianis, M.; Ferrari, E.; Ferry, S.; Froehlich, L.; Furlan, P.; Gaio, G.; Gelmetti, F.; Giannessi, L.; Giannini, M.; Gobessi, R.; Ivanov, R.; Karantzoulis, E.; Lonza, M.; Lutman, A.; Mahieu, B.; Milloch, M.; Milton, S.; Musardo, M.; Nikolov, I.; Noe, S.; Parmigiani, F.; Penco, G.; Petronio, M.; Pivetta, L.; Predonzani, M.; Rossi, F.; Rumiz, L.; Salom, A.; Scafuri, C.; Serpico, C.; Sigalotti, P.; Spampinati, S.; Spezzani, C.; Svandrlik, M.; Svetina, C.; Tazzari, S.; Trovo, M.; Umer, R.; Vascotto, A.; Veronese, M.; Visintini, R.; Zaccaria, M.; Zangrando, D.; Zangrando, M. *Nat. Photonics* **2012,** *6,* 699–704.
[23] LCLS Parameters, Website, 2015. https://portal.slac.stanford.edu/sites/lclscore_public/Accelerator_Physics_Published_Documents/LCLS-parameters.pdf.
[24] Bencivenga, F.; Baroni, S.; Carbone, C.; Chergui, M.; Danailov, M.B.; De Ninno, G.; Kiskinova, M.; Raimondi, L.; Svetina, C.; Masciovecchio, C. *New J. Phys*. **2013,** *15,* 123023-1–123023-27.
[25] Lee, D.; Albrecht, A.C. In *A Unified View of Raman, Resonance Raman and Fluorescence Spectroscopy*; Clark, R.J.H., Hester, R.E., Eds.; Advances in Infrared and Raman Spectroscopy, Vol. 12; Wiley Heyden: New York, 1985, pp 179–213.
[26] Patterson, B.D. Resource letter on stimulated inelastic X-ray scattering at an XFEL. SLAC Technical Note SLAC-TN-10-026; Menlo Park, CA: SLAC National Accelerator Laboratory, 2010.
[27] Krause, M.O. *J. Phys. Chem. Ref. Data* **1979,** *8,* 307–327.
[28] Gel'mukhanov, F.; Ågren, H. *Phys. Rep*. **1999,** *312,* 87–330.
[29] Bessy, II Parameters, Website, 2015. https://www.helmholtz-berlin.de/intern/nutzerplattform/betrieb-bessy/maschine/ring-parameter-tabelle_de.html.

[30] Bessy, II Beamlines, Website, 2015. http://www.helmholtz-berlin.de/user/beamtime/proposals/bessy-beamlines_de.html.

[31] Loudon, R. *The Quantum Theory of Light*; Oxford University Press, London, 1973.

[32] Boyd, R.W. *Radiometry and the Detection of Optical Radiation*; Wiley-Interscience: New York, 1983.

[33] Mehra, J.; Rechenberg, H. *Found. Phys.* **1999,** *29,* 91–132.

[34] Henke, B.L.; Gullikson, E.; Davis, J.C. *At. Data Nucl. Data Tables* **1993,** *54,* 181–342.

[35] Meystre, P.; Sargent III, M. *Elements of Quantum Optics*, 4th ed.; Springer-Verlag, Berlin Heidelberg, 2007.

[36] Liu, J.C.; Sun, Y.P.; Wang, C.K.; Ågren, H.; Gel'mukhanov, F. *Phys. Rev. A* **2010,** *81,* 1–7.

[37] Hubbell, J.H.; Trehan, P.N.; Singh, N.; Chand, B.; Mehta, D.; Garg, M.L.; Garg, R.R.; Singh, S.; Puri, S. *J. Phys. Chem. Ref. Data* **1994,** *23,* 339–364.

[38] Wernet, P.; Nordlund, D.; Bergmann, U.; Cavalleri, M.; Odelius, M.; Ogasawara, H.; Näslund, L.Å.; Hirsch, T.K.; Ojamäe, L.; Glatzel, P.; Pettersson, L.G.M.; Nilsson, A. *Science (New York, N.Y.)* **2004,** *304,* 995–999.

[39] Fuchs, O.; Zharnikov, M.; Weinhardt, L.; Blum, M.; Weigand, M.; Zubavichus, Y.; Bär, M.; Maier, F.; Denlinger, J.; Heske, C.; Grunze, M.; Umbach, E. *Phys. Rev. Lett.* **2008,** *100,* 027801-1–027801-4.

[40] Nilsson, A.; Tokushima, T.; Horikawa, Y.; Harada, Y.; Ljungberg, M.P.; Shin, S.; Pettersson, L.G. *J. Electron Spectrosc. Relat. Phenom.* **2013,** *188,* 84–100.

[41] Dell'Angela, M.; Anniyev, T.; Beye, M.; Coffee, R.; Föhlisch, A.; Gladh, J.; Katayama, T.; Kaya, S.; Krupin, O.; LaRue, J.; Møgelhøj, A.; Nordlund, D.; Nørskov, J.K.; Öberg, H.; Ogasawara, H.; Öström, H.; Pettersson, L.G.M.; Schlotter, W.F.; Sellberg, J.A.; Sorgenfrei, F.; Turner, J.J.; Wolf, M.; Wurth, W.; Nilsson, A. *Science (New York, N.Y.)* **2013,** *339,* 1302–1305.

[42] Öström, H.; Öberg, H.; Xin, H.; LaRue, J.; Beye, M.; Dell'Angela, M.; Gladh, J.; Ng, M.L.; Sellberg, J.A.; Kaya, S.; Mercurio, G.; Nordlund, D.; Hantschmann, M.; Hieke, F.; Kühn, D.; Schlotter, W.F.; Dakovski, G.L.; Turner, J.J.; Minitti, M.P.; Mitra, A.; Moeller, S.P.; Föhlisch, A.; Wolf, M.; Wurth, W.; Persson, M.; Nørskov, J.K.; Abild-Pedersen, F.; Ogasawara, H.; Pettersson, L.G.M.; Nilsson, A. *Science* **2015,** *347,* 978–982.

[43] Leinweber, P.; Kruse, J.; Walley, F.L.; Gillespie, A.; Eckhardt, K.U.; Blyth, R.I.R.; Regier, T. *J. Synchrotron Radiat.* **2007,** *14,* 500–511.

[44] Blum, M.; Odelius, M.; Weinhardt, L.; Pookpanratana, S.; Bär, M.; Zhang, Y.; Fuchs, O.; Yang, W.; Umbach, E.; Heske, C. *J. Phys. Chem. B* **2012,** *116,* 13757–13764.

[45] Mitzner, R.; Rehanek, J.; Kern, J.; Gul, S.; Hattne, J.; Taguchi, T.; Alonso-Mori, R.; Tran, R.; Weniger, C.; Schröder, H.; Quevedo, W.; Laksmono, H.; Sierra, R.G.; Han, G.; Lassalle-Kaiser, B.; Koroidov, S.; Kubicek, K.; Schreck, S.; Kunnus, K.; Brzhezinskaya, M.; Firsov, A.; Minitti, M.P.; Turner, J.J.; Moeller, S.; Sauter, N.K.; Bogan, M.J.; Nordlund, D.; Schlotter, W.F.; Messinger, J.; Borovik, A.; Techert, S.; De Groot, F.M.F.; Föhlisch, A.; Erko, A.; Bergmann, U.; Yachandra, V.K.; Wernet, P.; Yano, J. *J. Phys. Chem. Lett.* **2013,** *4,* 3641–3647.

[46] Wernet, P.; Kunnus, K.; Josefsson, I.; Rajkovic, I.; Quevedo, W.; Beye, M.; Schreck, S.; Grübel, S.; Scholz, M.; Nordlund, D.; Zhang, W.; Hartsock, R.W.; Schlotter, W.F.; Turner, J.J.; Kennedy, B.; Hennies, F.; de Groot, F.M.F.; Gaffney, K.J.; Techert, S.; Odelius, M.; Föhlisch, A. *Nature* **2015,** *520,* 78–81.

[47] Hendrickson, W.A.Q. *Rev. Biophys.* **2014,** *47,* 49–93.

[48] Kern, J.; Alonso-Mori, R.; Tran, R.; Hattne, J.; Gildea, R.J.; Echols, N.; Glöckner, C.; Hellmich, J.; Laksmono, H.; Sierra, R.G.; Lassalle-Kaiser, B.; Koroidov, S.; Lampe, A.; Han, G.; Gul, S.; Difiore, D.; Milathianaki, D.; Fry, A.R.; Miahnahri, A.; Schafer, D.W.; Messerschmidt, M.; Seibert, M.M.; Koglin, J.E.; Sokaras, D.; Weng, T.C.; Sellberg, J.; Latimer, M.J.; Grosse-Kunstleve, R.W.; Zwart, P.H.; White, W.E.; Glatzel, P.; Adams, P.D.; Bogan, M.J.; Williams, G.J.; Boutet, S.; Messinger, J.; Zouni, A.; Sauter, N.K.; Yachandra, V.K.; Bergmann, U.; Yano, J. *Science (New York, N.Y.)* **2013,** *340,* 491–495.

[49] Zhang, W.; Alonso-Mori, R.; Bergmann, U.; Bressler, C.; Chollet, M.; Galler, A.; Gawelda, W.; Hadt, R.G.; Hartsock, R.W.; Kroll, T.; Kjær, K.S.; Kubiček, K.; Lemke, H.T.; Liang, H.W.; Meyer, D.A.; Nielsen, M.M.; Purser, C.; Robinson, J.S.; Solomon, E.I.; Sun, Z.; Sokaras, D.; van Driel, T.B.; Vankó, G.; Weng, T.C.; Zhu, D.; Gaffney, K.J. *Nature* **2014,** *509,* 345–348.

[50] Chapman, H.N.; Nugent, K.A. *Nat. Photonics* **2010,** *4,* 833–839.

[51] Amann, J.; Berg, W.; Blank, V.; Decker, F.J.; Ding, Y.; Emma, P.; Feng, Y.; Frisch, J.; Fritz, D.; Hastings, J.; Huang, Z.; Krzywinski, J.; Lindberg, R.; Loos, H.; Lutman, A.; Nuhn, H.D.; Ratner, D.; Rzepiela, J.; Shu, D.; Shvyd'ko, Y.; Spampinati, S.; Stoupin, S.; Terentyev, S.; Trakhtenberg, E.; Walz, D.; Welch, J.; Wu, J.; Zholents, A.; Zhu, D. *Nat. Photonics* **2012,** *6,* 693–698.

[52] Castagna, J.C.; Murphy, B.; Bozek, J.; Berrah, N. *J. Phys.: Conf. Ser.* **2013,** *425,* 152021-1–152021-5.

[53] Murphy, B.F.; Castagna, J.C.; Bozek, J.D.; Berrah, N. In *Mirror-based Soft X-ray Split-and-delay System for Femtosecond Pump-probe Experiments at LCLS*, X-ray Free-electron Lasers: Beam Diagnostics, Beamline Instrumentation, and Applications; Moeller, S.P., Yabashi, M., Hau-Riege, S.P., Eds; San Diego, CA, 2012; Vol. 8504; p. 850409.

[54] Corkum, P. *Phys. Rev. Lett.* **1993,** *71,* 1994–1997.

[55] Midorikawa, K. *Jpn. J. Appl. Phys.* **2011,** *50,* 090001-1–090001-12.

[56] Popmintchev, T.; Chen, M.C.; Arpin, P.; Murnane, M.M.; Kapteyn, H.C. *Nat. Photonics* **2010,** *4,* 822–832.

[57] Popmintchev, T.; Chen, M.C.; Popmintchev, D.; Arpin, P.; Brown, S.; Alisauskas, S.; Andriukaitis, G.; Balciunas, T.; Mücke, O.D.; Pugzlys, A.; Baltuska, A.; Shim, B.; Schrauth, S.E.; Gaeta, A.; Hernández-García, C.; Plaja, L.; Becker, A.; Jaron-Becker, A.; Murnane, M.M.; Kapteyn, H.C. *Science (New York, N.Y.)* **2012,** *336,* 1287–1291.

[58] Thompson, A.C.; Attwood, D.T.; Gullikson, E.M.; Howells, M.R.; Kortright, J.B.; Robinson, A.L.; Underwood, J.H.; Kim, K.J.; Kirz, J.; Lindau, I.; Pianetta, P.; Winick, H.; Williams, G.P.; Scofield, J.H. *X-ray Data Booklet*; Lawrence Berkeley National Laboratory, Berkeley, 2009.

[59] Barty, A.; Caleman, C.; Aquila, A.; Timneanu, N.; Lomb, L.; White, T.A.; Andreasson, J.; Arnlund, D.; Bajt, S.; Barends, T.R.M.; Barthelmess, M.; Bogan, M.J.; Bostedt, C.; Bozek, J.D.; Coffee, R.; Coppola, N.; Davidsson, J.; DePonte, D.P.; Doak, R.B.; Ekeberg, T.; Elser, V.; Epp, S.W.; Erk, B.; Fleckenstein, H.; Foucar, L.; Fromme, P.; Graafsma, H.; Gumprecht, L.; Hajdu, J.; Hampton, C.Y.; Hartmann, R.; Hartmann, A.; Hauser, G.; Hirsemann, H.; Holl, P.; Hunter, M.S.; Johansson, L.; Kassemeyer, S.; Kimmel, N.; Kirian, R.A.; Liang, M.; Maia, F.R.N.C.; Malmerberg, E.; Marchesini, S.; Martin, A.V.; Nass, K.; Neutze, R.; Reich, C.; Rolles, D.; Rudek, B.; Rudenko, A.; Scott, H.; Schlichting, I.; Schulz, J.; Seibert, M.M.; Shoeman, R.L.; Sierra, R.G.; Soltau, H.; Spence, J.C.H.; Stellato, F.; Stern, S.; Strüder, L.; Ullrich, J.; Wang, X.; Weidenspointner, G.; Weierstall, U.; Wunderer, C.B.; Chapman, H.N. *Nat. Photonics* **2011,** *6,* 35–40.